

## ORIGINAL ARTICLE

# iPS cells from Chediak-Higashi syndrome patients recapitulate the giant granules in myeloid cells

Shigeharu Oh<sup>1</sup> | Akira Niwa<sup>1</sup>  | Ayako Nagahashi<sup>2</sup> | Isao Asaka<sup>2</sup> |  
Tatsutoshi Nakahata<sup>1,2</sup> | Megumu K. Saito<sup>1</sup> 

<sup>1</sup>Department of Clinical Application, Center for iPS Cell Research and Application, Kyoto University, Kyoto, Japan

<sup>2</sup>Department of Fundamental Cell Technologies, Center for iPS Cell Research and Application, Kyoto University, Kyoto, Japan

**Correspondence**

Akira Niwa and Megumu K. Saito, Department of Clinical Application, Center for iPS Cell Research and Application (CiRA), Kyoto University, 53, Shogoin-Kawahara-cho, Sakyo-ku, Kyoto, Japan.

Email: [akiranw@cira.kyoto-u.ac.jp](mailto:akiranw@cira.kyoto-u.ac.jp) and [msaito@cira.kyoto-u.ac.jp](mailto:msaito@cira.kyoto-u.ac.jp)

**Present address**

Shigeharu Oh, Department of Pediatrics, Valstagarde Hospital, Nara, Japan

Ayako Nagahashi, RIKEN Center for Advanced Intelligence Project Medical-risk Avoidance Based on iPS Cells Team, Kyoto, Japan

Tatsutoshi Nakahata, Central Institute for Experimental Animals, Kawasaki, Japan

**Funding information**

Japan Agency for Medical Research and Development, Grant/Award Number: 21bm0804004, JP19bm0804001 and JP21bm0104001; Japan Society for the Promotion of Science, Grant/Award Number: 20H03642

## INTRODUCTION

Chediak-Higashi syndrome (CHS; MIM214500) is a rare autosomal recessive congenital immunodeficiency caused by mutations in the lysosomal trafficking regulator (*LYST*) gene.<sup>1-3</sup> Patients suffer from persistent and recurrent bacterial infections of the skin, mucous membranes, and respiratory tract. Other symptoms include hemophagocytic lymphohistiocytosis (HLH), oculocutaneous albinism, bleeding tendency, and late-onset progressive neurological symptoms. An important cellular feature is the presence of giant granules in peripheral blood leukocytes.

**Abstract**

**Background:** Chediak-Higashi syndrome (CHS) is a congenital disease characterized by immunodeficiency, hemophagocytic lymphohistiocytosis, oculocutaneous albinism, and neurological symptoms. The presence of giant granules in peripheral blood leukocytes is an important hallmark of CHS. Here we prepared induced pluripotent stem cells (iPSCs) from CHS patients (CHS-iPSCs) and differentiated them into hematopoietic cells to model the disease phenotypes.

**Methods:** Fibroblasts were obtained from two CHS patients and then reprogrammed into iPSCs. The iPSCs were differentiated into myeloid cells; the size of the cytosolic granules was quantified by May-Grunwald Giemsa staining and myeloperoxidase staining.

**Results:** Two clones of iPSCs were established from each patient. The differentiation efficiency to CD33<sup>+</sup>CD45<sup>+</sup> myeloid cells was not significantly different in CHS-iPSCs compared with control iPSCs, but significantly larger granules were observed.

**Conclusions:** We succeeded in reproducing a characteristic cellular phenotype, giant granules in myeloid cells, using CHS-iPSCs, demonstrating that iPSCs can be used to model the pathogenesis of CHS patients.

**KEYWORDS**

Chediak-Higashi syndrome, induced pluripotent stem cells, myeloid cells

The lysosomal trafficking regulator localizes lysosomes and regulates the size and quality of lysosomes. At the same time, enlarged lysosomes are observed in *LYST*-depleted cells.<sup>4</sup> *LYST* is also involved in the degranulation of cytotoxic T lymphocytes (CTLs) to exert cytotoxicity,<sup>5</sup> is linked to endo-lysosomal organization and mediates toll-like receptor 3 (TLR3)- and TLR4-associated proinflammatory signaling.<sup>6</sup> Dysfunction of these lysosome-associated signaling responses is thought to be responsible for the onset of immunodeficiency and HLH. On the other hand, myeloid cells, especially neutrophils, store a specific peroxidase, myeloperoxidase (MPO) in their azurophilic granules. MPO is released

extracellularly or into phagolysosomes and exerts a bactericidal capacity.<sup>7</sup> The presence of MPO-positive giant granules in neutrophils is one of the main hallmarks of CHS.<sup>8</sup>

In addition to susceptibility to infection due to immunodeficiency, CHS is often complicated by HLH, an immunological hyperactive condition that can be fatal.<sup>9</sup> The onset of HLH in CHS represents the accelerated phase and occurs in most CHS patients.<sup>10</sup> Since the accelerated phase and immunodeficiency are the most important causes of death in CHS patients,<sup>11</sup> hematopoietic stem cell transplantation (HSCT) has been performed.<sup>12–15</sup>

However, the outcome of HST is poor, with an overall survival rate of around 60%–75%,<sup>12–15</sup> and the prognosis is even worse for patients in the accelerated phase.<sup>13</sup> In addition, phenotypes other than those of the immune system are not recovered by HSCT. For example, for photosensitivity due to oculocutaneous albinism, supportive care is needed even after transplantation. Furthermore, in a study, all CHS patients who underwent HSCT showed neurological deficits or low cognitive abilities in long-term observation.<sup>16</sup> Since HSCT cannot prevent the long-term deterioration of patients' quality of life due to these neurodegenerative symptoms, curative alternative treatment options are needed.

Animal models have been used to study CHS, but they do not completely reproduce the human phenotype<sup>17</sup> and differ in many aspects from the human immune system.<sup>18</sup> An alternative approach for the development of therapies for rare genetic diseases is the use of induced pluripotent stem cells (iPSCs).<sup>19,20</sup> In vitro phenotyping of iPSCs by differentiating them into various types of cells is useful for pathological and therapeutic analysis. Several studies have generated iPSCs from CHS patients (CHS-iPSCs).<sup>21–23</sup> Although one report described the differentiation of CHS-iPSCs into melanocytes and reported that the size of melanosomes increased,<sup>22</sup> the differentiation of CHS-iPSCs to immune cells has not been reported. In this report, we differentiated CHS patient-derived iPSCs into myeloid cells and measured the size of intracellular granules to verify whether iPSC-derived blood cells can reproduce the pathology.

## METHODS

### Ethical approval

This study was approved by the ethics committee of Kyoto University and Shizuoka Children's Hospital, Japan (R0091). Written informed consent was obtained from the patients' guardians in accordance with the Declaration of Helsinki. The use of human embryonic stem cells (ESCs) was approved by the Ministry of Education Culture, Sports, Science and Technology (MEXT) of Japan.

## Human pluripotent stem cell (PSC) lines

A human ESC line, KhES1, was kindly provided by Dr. Norio Nakatsuji (Kyoto University). An iPSC line, 201B7, was kindly provided by Dr. Shinya Yamanaka (Kyoto University).<sup>24</sup>

## Patients

Patient CIRA00150 was a Japanese girl aged 7 years when recruited. Her clinical course and genetic diagnosis have been described previously.<sup>25</sup> In brief, at the age of 4, she developed cough, rhinorrhea, and high fever and was admitted to hospital because of persistent symptoms and pancytopenia. She was diagnosed with CHS with HLH on the basis of clinical features (silvery hair, light skin, photosensitivity, astigmatism, and amblyopia) and laboratory findings (giant granules in white blood cells, hemophagocytosis, and defective cytotoxicity of peripheral mononuclear cells against K562 cells). She successfully received HSCT, and there were no manifestations of giant granules in white blood cells, HLH, recurrent infections, dysautonomia, cerebellar symptoms, or involuntary movements thereafter. At 5 years old, the Wechsler Intelligence Scale for Children-Third edition showed a score of 68 for verbal intelligence quotient (IQ), 90 for the performance IQ, and 76 for the full-scale IQ score. T2-weighted-fluid-attenuated inversion recovery brain magnetic resonance imaging showed a high intensity signal in the bilateral white matter of the cerebrum.

The second patient, CIRA00153, was originally registered as GM02075 in the repository of the Coriell Institute and renamed according to the institutional rule.<sup>2</sup> The donor of GM02075 fibroblasts was a 1-year-old Caucasian girl. Her clinical features included photophobia, cytoplasmic inclusions in white blood cells, and partial oculocutaneous albinism. No susceptibilities to infection, HLH, or neurological impairments were noted.

## Human iPSC establishment

Fibroblasts from the two patients (CIRA00150 and CIRA00153) were cultured in Dulbecco's Modified Eagle's Medium (Nacalai Tesque) containing 10% fetal bovine serum (Hyclone). Reprogramming was performed by introducing episomal plasmid vectors carrying *OCT3/4*, *SOX2*, *KLF4*, *LIN28A*, *L-MYC* and *shp53*, as previously described.<sup>26</sup> Dr. Keisuke Okita (Kyoto University) kindly provided the plasmids. Six days after the transduction, the cells were harvested and replated onto mitotically inactivated SNL feeder cells. The next day, the medium was replaced with Primate ES cell medium (ReproCELL) supplemented with 5 ng/ml bFGF (Wako). Three weeks after, individual colonies were

isolated and expanded. Cell culture was performed at 37°C, 5% CO<sub>2</sub>, and 21% O<sub>2</sub>. Cell morphology was observed using an Olympus CKX31 inverted microscope. Sample images were acquired using a BIOREVO BZ-X700 fluorescence microscope (Keyence).

## Genetic analysis

Genomic DNA from the fibroblasts was isolated using a QIAamp DNA Blood Mini Kit (Qiagen), according to the manufacturer's protocol. Polymerase chain reaction (PCR) primer pairs designed from the sequences around exons 3 and 10 were used to amplify genomic DNA segments. Exons 9–10 were amplified using the forward primer 5'-AGCCAAACTTGATGTGCTTGCCC-3' and reverse primer 5'-ACCAGATATGGCAACAACATGGCA-3'; exon 3 was amplified using the forward primer 5'-CCTATTCTCAGCTATGCTCAGGT-3' and reverse primer 5'-GCTTTCCTCCAGAATTAGCAGC-3'. PCR was performed using PrimeSTAR GXL DNA Polymerase (Takara), according to the manufacturer's protocol. The PCR products of exons 3 and 10 of *LYST* were purified using the Gel/PCR DNA Isolation System (Viogene) and sequenced directly using an ABI 3500 sequencer (Applied Biosystems).

## Karyotyping

Karyotyping was performed by G-banding (Nihon Gene Research Laboratories Inc.) or Q-banding (Chromocenter Inc.) to examine the integrity of the chromosomes.

## Quantitative reverse transcription polymerase chain reaction (RT-qPCR) for the detection of transgene sequences

Genomic DNA from iPSCs was isolated using the QIAamp DNA Blood Mini Kit, according to the manufacturer's protocol. Transgene sequences were detected by RT-qPCR (TaqMan® Gene Expression Assays) for detection of CAG promoter, *OCT3/4*, *KLF4*, *SOX2*, *EBNA-1*, *LIN28A* and *LMYC*, according to the manufacturer's protocol. Each well contained 50 ng of genomic DNA. Standard curves were obtained by serial dilutions of plasmids (pCXLE-hOCT3/4-shp53, pCXLE-hSK, which contains the *SOX2* and *KLF4* sequences, and pCXLE-hUL, which contains the *LIN28A* and *LMYC* sequences). The number of integrated vector copy numbers per cell was determined by the observed cycle threshold values. All primers and probes were obtained from Applied Biosystems. The sequence of each primer is shown as follows. 7CAG promoter: forward

primer, 5'-GGCTCTGACTGACCGCGTTA-3', and reverse primer, 5'-AATGCACGGCTAGGGTCAAA-3'; *OCT3/4*: forward primer, 5'-TGTCTCATCATTTTGGCA AAGAATT-3', and reverse primer, 5'-CGAGAAGGCG AAATCCGAA-3'; *KLF4*: Hs00358836\_m1; *SOX2*: forward primer, 5'-GAATTGTT CATGA GTGGACCTG G-3', and reverse primer, 5'-GAATTGTT CATGAGT GGACCTGG-3'; *EBNA-1*: forward primer, 5'-ATC AGGGCCAAG ACATAGAGATG-3', and reverse primer, 5'-GCCAATGCAACTTGGACGTT-3'; *LIN28A*: forward primer, 5'-CAAAAGGAAAGAG CATGCAG AA-3', and reverse primer, 5'-CATGATGATCTAGACC TCCACAGTTG-3'; and *LMYC*: Hs00420495\_m1.

## Teratoma assay

Teratoma assays were performed as described previously.<sup>27</sup> Briefly, approximately 2 × 10<sup>6</sup> iPSCs were injected subcutaneously into the dorsal flank of immunocompromised NOD/scid/ $\gamma$ c<sup>null</sup> mice (Central Institute for Experimental Animals, Japan). Masses were excised 8–12 weeks after the injection. Paraffin-embedded tissues were sliced and stained with hematoxylin and eosin. Sample images were acquired using a BIOREVO BZ-9000 fluorescence microscope.

## In vitro differentiation into myeloid cells

Myeloid differentiation was performed based on previous protocols.<sup>28,29</sup> In brief, human PSCs were maintained on iMatrix (Nippi)-coated plates with StemFit (Ajinomoto) medium, according to the manufacturer's protocol.<sup>30</sup> First, undifferentiated PSCs were passaged at a density of 3000 cells per well in a 6-well tissue culture plate coated with growth factor reduced Matrigel (Corning) previously diluted 50-fold in phosphate-buffered saline (PBS) (-). When individual colonies grew up to approximately 500 μm in diameter, mTeSR1 maintenance medium (Stem Cell Technology) was replaced with mTeSR1 medium that contained BMP4 (80 ng/μl; R&D systems). This day this occurred was defined as day 0 of differentiation. During the differentiation to myeloid cells, the cells were cultured at 37°C, 5% CO<sub>2</sub>, and 5% O<sub>2</sub>. On day 4, the mTeSR1 medium was replaced with StemPro34 (Life Technologies) that contained L-glutamine (2 mM; Gibco), VEGFA (80 ng/μl; R&D systems), SCF (100 ng/μl; R&D systems), and FGF2 (25 ng/μl; R&D systems). On day 6, the medium was replaced with StemPro3, that contained L-glutamine (2 mM), SCF (50 ng/μl; R&D systems), IL-3 (50 ng/μl; R&D systems), and G-CSF (50 ng/μl; R&D systems). On day 10, the medium was replaced with StemPro34 that contained L-glutamine (2 mM), SCF (50 ng/μl; R&D systems), and G-CSF (50 ng/μl; R&D

Systems). Thereafter, the medium was replaced every 5 days.

### Flowcytometric analysis

The adherent cells (days 6 and 10) were treated with Accumax (Innovative Cell Technologies) and harvested by scraping the culture dish. Floating cells were harvested with culture medium on days 15, 20, and 25. Cells were treated with FcR Blocking Reagent, Human (Miltenyi Biotec, 130–059-901). Isotype controls were obtained using FITC Mouse IgG1 k Isotype Control Antibody (BioLegend, 400110), PE Mouse IgG1 k Isotype Control Antibody (BioLegend, 400114), and APC Mouse IgG1 k Isotype Control Antibody (BioLegend, 400122). Cells were stained by KDR-APC (BioLegend, 338909), CD33-PE (Beckton Dickinson, 347787), CD34-PE (Beckman Coulter, A07776), CD43-FITC (eBioscience, 315203), and CD45-APC (IOtest, IM2473), according to the manufacturer's protocol. Samples were analyzed using a MACSQuant Analyzer (Miltenyi Biotec) and FlowJo software (Thermo).

### May-Grunwald Giemsa staining

Floating cells were centrifuged onto glass slides using a Shandon Cytospin4 Cytocentrifuge (Thermo Scientific). Samples were fixed for 30 s at room temperature in May-Grunwald solution (Merck) and then washed for 30 s with gently running tap water. The stained preparations were counterstained in freshly prepared Giemsa stain solution (Merck) diluted 5-fold in water for 10 min. Sample images were acquired using the BIOREVO BZ-9000 fluorescence microscope.

### MPO staining

Floating cells were centrifuged onto glass slides using the Shandon Cytospin4 Cytocentrifuge. MPO staining was performed using a DAB staining kit (Muto Pure Chemicals), according to the manufacturer's protocol. The samples were fixed with 82% ethanol +2.5% glutaraldehyde at room temperature for 30 s and washed for 30 s with gently running tap water. Then, the incubation mixture (0.5 mg/ml diaminobenzidine, 5 ml Tris–HCL buffer [0.587% Tris, 0.1% HCL], and 0.1 ml 3% hydrogen peroxide) was put on glass slides for 5 min at room temperature and washed for 30 s with gently running tap water. Finally, the stained preparations were counterstained in freshly prepared Giemsa stain solution diluted 5-fold in water for 10 min. These preparations were photographed and analyzed using the BIOREVO BZ-9000 fluorescence microscope. The area of the maximum MPO positive granules in each myeloid cell was measured in a blinded manner.

### MPO electron microscopy

Cells were fixed in 1.25% glutaraldehyde and 2% paraformaldehyde in PBS (–) for 1 h at room temperature. Then they were put into two incubation mixtures sequentially for 30 min (incubation mixture 1: 0.5 mg/ml diaminobenzidine and 0.05 M Tris–HCL buffer; incubation mixture 2: 0.01% hydrogen peroxide and 1 ml 0.05 M Tris–HCL buffer) and fixed in 1% osmium tetroxide in PBS (–) for 2 h. After fixation, the samples were dehydrated in a graded ethanol series, cleaned up with propylene oxide and embedded in Epon (Nacalai Tesque). Thin sections were stained by uranyl acetate and Reynolds lead citrate and examined using a transmission electron microscope (H7650, Hitachi).

### RNA extraction and RT-qPCR analysis for the detection of myeloid cell-associated genes

RNA samples were prepared using silica gel membrane-based spin-columns (RNAeasy Kit), following the manufacturer's instructions, then subjected to reverse transcription using the PrimeScript™ RT Master Mix (Takara) to obtain cDNA. The expression of myeloid cell-associated genes, including *LYST*, *SPII*, *MPO*, *LAMP1*, and *CEBPA*, were then quantified using RT-PCR with TB Green® Premix Ex Taq™ (Tli RnaseH Plus) (Takara) and the following primer pairs: *LYST* (NM\_000081): 5'-GATCTCTCAGGTCTTCTGGTTTC-3' (Sense) and 5'-CAGCACCGCTCAGGATAATAA-3' (Antisense); *SPII* (NM\_003120): 5'-CGACATGA AGGACAGC ATCT-3' (Sense) and 5'-GCCATCTTC TGGTAGGTC ATC-3' (Antisense); *MPO* (NM\_000250): 5'-GCAT CTGAGAGAAGAGAAGAAGG-3' (Sense) and 5'-GCATCTGAGAGAAGAGAAGAAGG-3' (Antisense); *LAMP1* (NM\_005561): 5'-CGTCAGCAGCAATGTT TATGG-3' (Sense) and 5'-CATGTTCTTAGGGCC ACTCTT-3' (Antisense); *CEBPA* (NM\_001287424.2): 5'-AGAACAGCAACGAG TACCGG-3' (Sense) and 5'-GCGGTCATTGTC ACT GGTCA-3' (Antisense); and *ACTB* (NM\_001101.5s): 5'-GTCATT CCAAATATG AGATGCGT-3' (Sense) and 5'-GCTATCACC TCCCCT GTGTG-3' (Antisense). Thermal cycling was performed on Step-One Plus (Applied Biosystems) with the following parameters: 95°C for 5 min, then 40 cycles of 95°C for 5 s, and 60°C for 60 s.

### Statistical analysis

Statistical analyses were performed using GraphPad Prism, version 6.0 (GraphPad Software). Graphs were generated using GraphPad Prism version 6.0, Excel and PowerPoint (Microsoft). Results are shown as means and standard errors of the means. Comparisons between groups were performed using the Kruskal-Wallis one-way analysis of variance with Dunn's

multiple comparisons test. Significance was defined as  $p < 0.05$ .

## RESULTS

### Generation of iPSCs from two patients with CHS with heterozygous *LYST* mutations

We first established multiple iPSC lines by introducing episomal plasmid vectors carrying *OCT3/4*, *SOX2*, *KLF4*, *shp53*, *LIN28A*, and *L-MYC*<sup>31</sup> into fibroblasts obtained from two patients with CHS (CIRA00150 and CIRA00153). Fibroblasts from both patients had heterozygous frameshift mutations at different positions in the ARM/HEAT repeat domain of *LYST* as previously described (CIRA00153:c.118\_119insG, p.A40fsx63<sup>25</sup>; CIRA00150:c.3944\_3945insC, p.T1315fsX1331<sup>2</sup>; Figure 1a,b). We picked up two iPSC colonies per patient after reprogramming and used them for the subsequent analysis (CIRA00150-19, CIRA00150-22, CIRA00153-9 and CIRA00153-18). The CHS-iPSCs exhibited typical undifferentiated PSC-like morphology (Figure 1c). The copy numbers of the residual transgenes derived from the episomal plasmid vectors were negligible (Table S1). All clones exhibited normal karyotype (Figure S1). All CHS-iPSCs formed derivatives of all three germ layers by the teratoma formation assay (Figure 1d).

### Myeloid cell differentiation from CHS-iPSCs

Next, the CHS-iPSCs and control PSCs (201B7 and KhES1) were differentiated into myeloid cells using a previously described feeder- and serum-free monolayer culture with some modification. To focus more on neutrophil differentiation, G-CSF was here used as the core hematopoietic cytokine instead of GM-CSF and M-CSF used in original method (Figure 2a).<sup>28,29</sup> In accordance with previously reported stepwise differentiation,<sup>28,29</sup> the iPSCs (negative for KDR or CD34) were initially committed into KDR-positive mesodermal progenitors including CD34<sup>+</sup>KDR<sup>+</sup> hemoangiogenic progenitors that give rise to hematopoietic cells and are subsequently differentiated into CD43<sup>+</sup> hematopoietic progenitor cells and CD45<sup>+</sup>CD33<sup>+</sup> myeloid cells (Figure 2b). We noticed variations in the differentiation efficacy, to some extent, at the stage of hemoangiogenic progenitor cells and hematopoietic progenitor cells, especially a lower efficiency in CIRA00153-18 (Figure 2c). Nevertheless, by subsequent differentiation, the CD33<sup>+</sup>CD45<sup>+</sup> myeloid cells were continuously recovered with comparable efficiency from all evaluated iPSC clones (Figure 2d). We here describe those cells as “Myelocytes” because it is difficult to completely exclude contaminated immature myeloid lineage cells, though many of the cells recovered were consistent with mature neutrophils (data not shown). From these observations, we concluded that

disease-associated *LYST* mutations do not affect the efficiency of myeloid differentiation from human iPSCs.

### Expression of myeloid-associated genes in CHS-iPSCs

To confirm the validity of myeloid differentiation, we verified the expression of myeloid-associated genes during the differentiation (Figure 3). As expected, genes expressed in myeloid cells, such as *SPI1*, *MPO* and *CEBPA*, were upregulated in day-20 myeloid cells, while a lysosomal membrane-associated gene, *LAMP1*, was constitutively expressed. *LYST* was also upregulated in day-20 myeloid cells and maintained even in patient-derived clones.

### Recapitulation of cytosolic giant granules in myeloid cells from CHS-iPSCs

We next evaluated the formation of cytosolic giant granules in the myeloid cells derived from CHS-iPSCs (Figure 4a) because these granules are an important hallmark of CHS patient hematopoietic cells.<sup>8</sup> Hematopoietic cells harvested on days 15–25 of the differentiation presented morphologies characteristic of myeloid cells, such as a horseshoe-shaped or segmented nucleus, pale blue to pink cytoplasm, and granules in the cytoplasm (Figure 4b). Some of the cytoplasmic granules were also positive for MPO staining (Figure 4b, right panel). These cytosolic giant granules were clearly observed in all CHS-iPSC-derived myeloid cells at each time point and positive for MPO, confirming that they were lysosomes or phagolysosomes.<sup>7</sup> The area of the maximum MPO-positive granules in the cells derived from the CHS-iPSC lines were significantly larger than those derived from wild type controls (Figure 4c). Interestingly, not all CHS-iPSC-derived myeloid cells had large granules, and others had huge granules.

In addition, electron microscopy showed MPO-positive giant granules and cytoplasmic vacuoles, which is characteristic morphology of CHS<sup>32,33</sup> (Figure 4d). Taken together, these results demonstrate that differentiated iPSC-derived myeloid cells successfully recapitulated the abnormal morphologies of myeloid cells in CHS.

## DISCUSSION

In this report, we differentiated CHS patient-derived iPSCs into myeloid cells, measured their granule size, and observed giant granules in hematopoietic cells derived from the myeloid cells, an important hallmark of CHS. At the mRNA level, *LYST* expression was slightly different among clones from the same patient. However, none of the patient-derived clones lost more than half

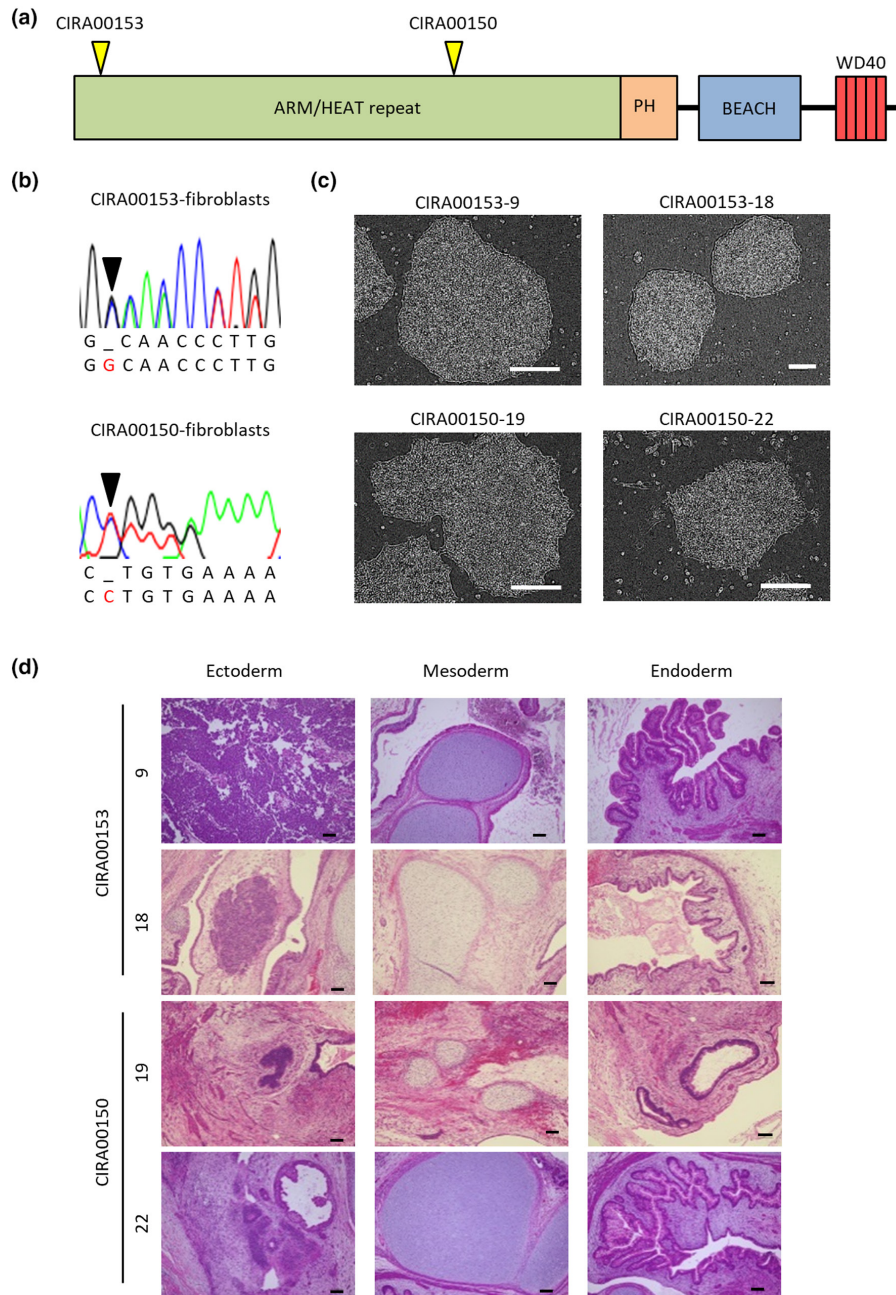


**FIGURE 1** Generation and characterization of Chediak-Higashi syndrome induced pluripotent stem cells (CHS-iPSCs). (a) Domain structure of the *LYST* gene and the sites of mutations observed in the patients. (b) Chromatogram of direct sequencing of genomic DNA obtained from fibroblasts. (c) Bright field images of CHS-iPSC clones. Bars = 100  $\mu$ m. (d) Teratoma formation assay. Bars = 100  $\mu$ m.

of their *LYST* expression. This result contrasted with our expectation because mutant alleles with premature stop codons should decay via the nonsense-mediated RNA decay (NMD) mechanism. Although the extent of NMD involvement in our data is unclear, there may be a compensatory increase in gene expression from normal alleles.

Interestingly, despite the comparable expression of *LYST* gene, the size of the granules was different between patients (Figure 4c). This difference was not associated with clonal variation, because the maximum size of the granules was consistent between the clones derived from

same patient. Both patients were found to have only a single allele frameshift mutation in *LYST*. It is possible then that there is an undiscovered *LYST* mutation on the other allele that affects the *LYST* function and granule size of myeloid cells. Another possibility is that mutations in other modifier genes may also be responsible for the phenotypic difference. However, since there is no report showing that myeloid cell granule size in CHS is associated with disease severity, the clinical significance of this finding needs to be carefully evaluated in the future.

On the other hand, the granule size of individual myeloid cells differentiated from CHS-iPSCs showed

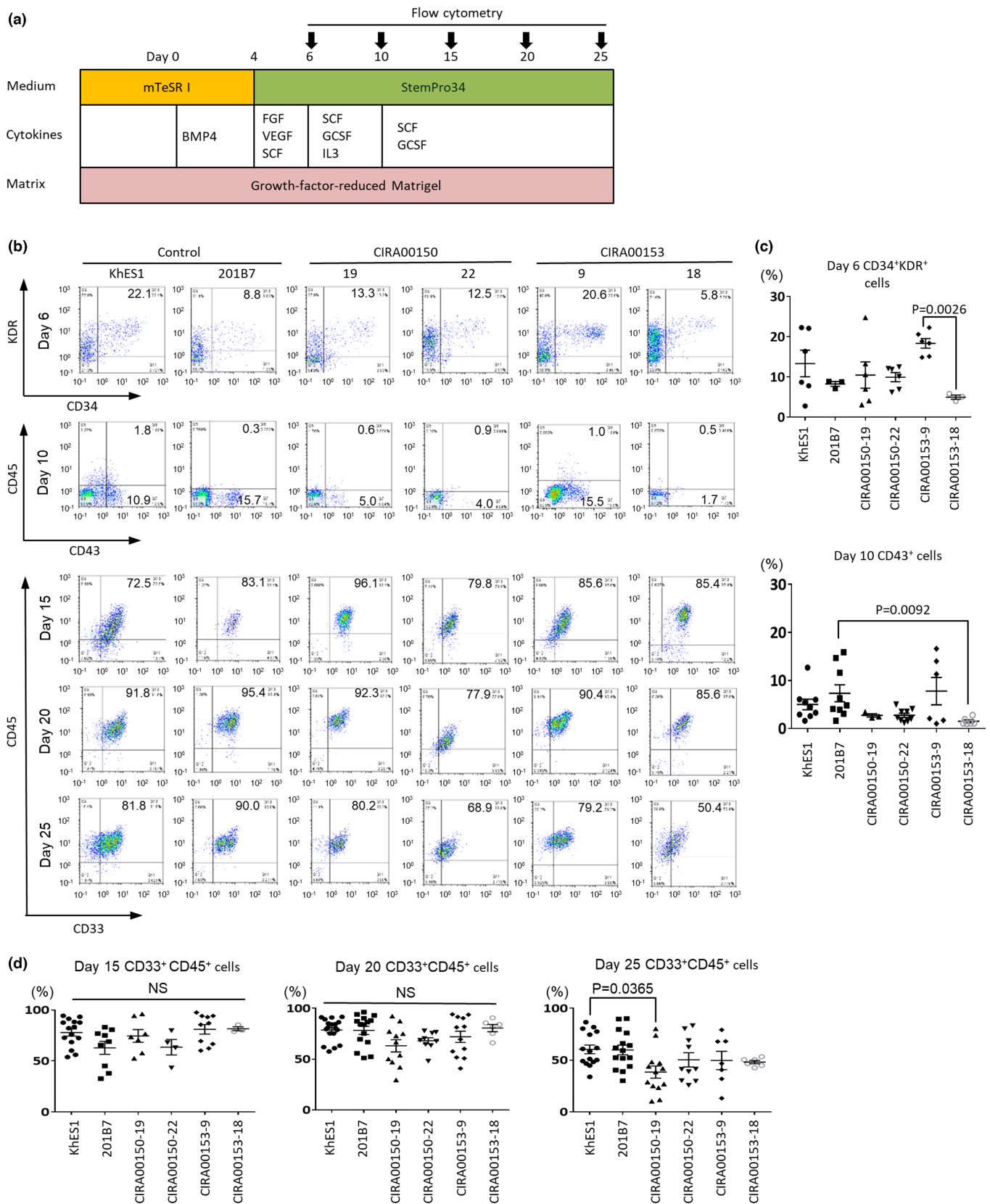


**FIGURE 2** Myeloid differentiation potential of Chediak-Higashi syndrome induced pluripotent stem cells. (a) Schematic diagram of myeloid cell differentiation and analysis. (b) Representative flow cytogram for myeloid cell differentiation. (c) Percentage of day 6 CD34<sup>+</sup>KDR<sup>+</sup> hemoangiogenic progenitor cells and day 10 CD43<sup>+</sup> hematopoietic progenitor cells. Individual experimental attempts (n = 3–9) are plotted in the graphs. (d) Percentage of CD33<sup>+</sup>CD45<sup>+</sup> myeloid cells. Individual experimental attempts (n = 3–18) are plotted in the graphs. Each bar represents the mean and the standard error of the mean from multiple independent experiments. Statistical analysis was performed using the Kruskal-Wallis one-way analysis of variance with Dunn's multiple comparisons test. NS, not significant.

a wide distribution, ranging from giant to normal sizes. In a study using patient-derived natural killer (NK) cells and CTLs, some cells with normal cytotoxic

granule size were also observed.<sup>34</sup> Studies using CHS fibroblasts have reported that the localization of intracellular granules is different between CHS and healthy

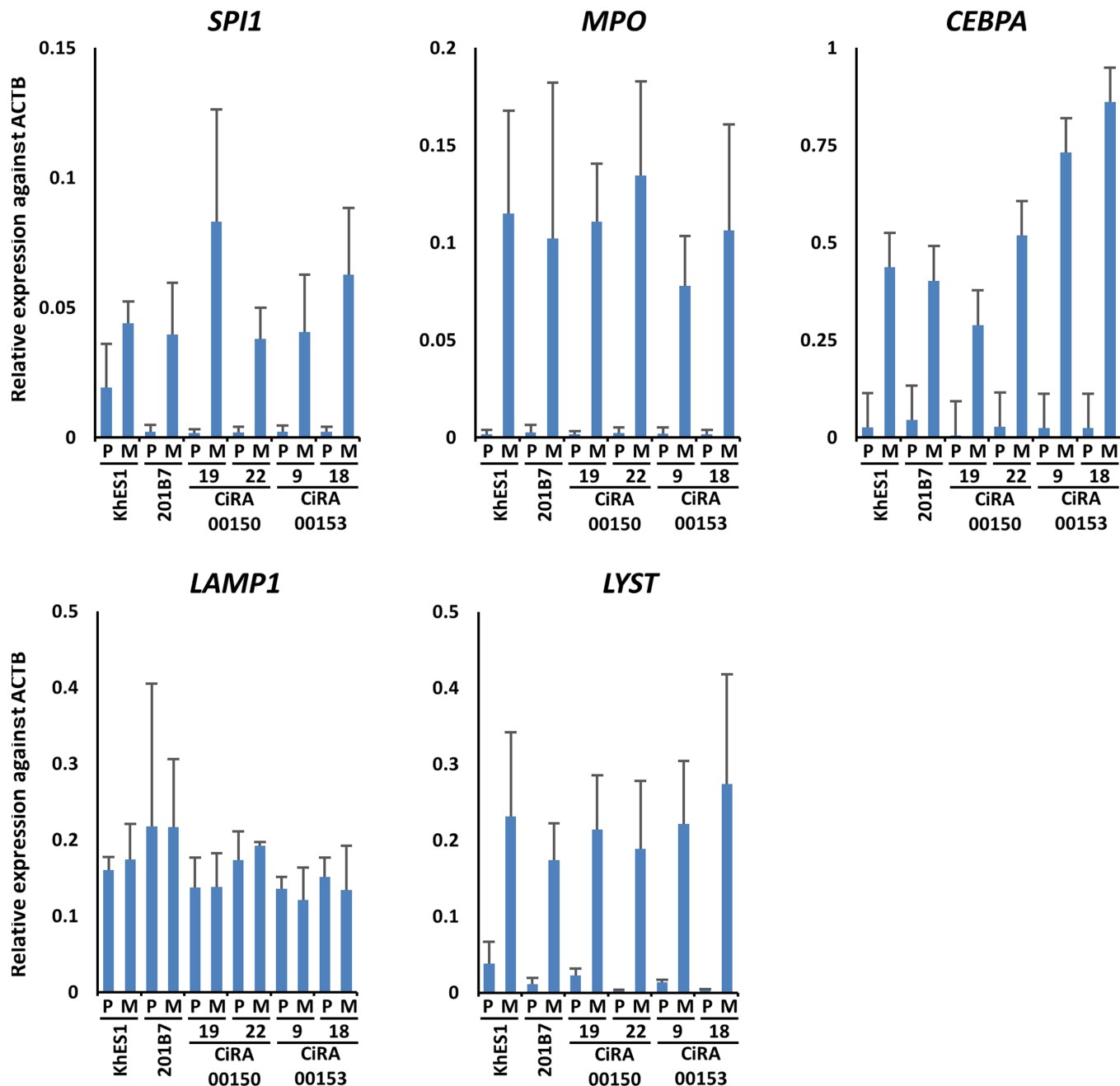
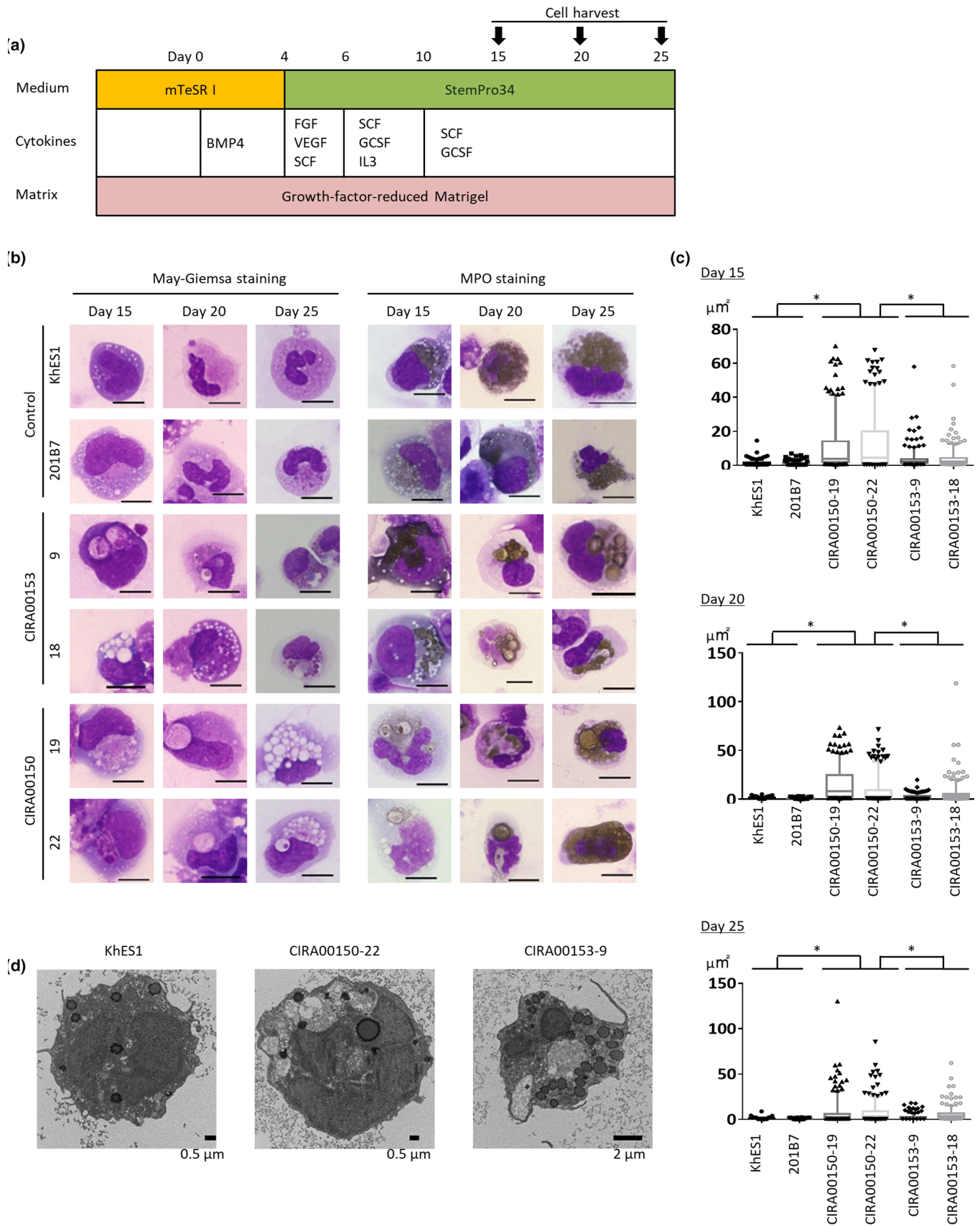


**FIGURE 3** Expression of myeloid-associated genes in Chediak-Higashi syndrome induced pluripotent stem cell-derived myeloid cells. Gene expression was evaluated using real time polymerase chain reaction analysis. RNA was isolated from undifferentiated pluripotent stem cells (P) and differentiated myeloid cells on day 20 (M). The values on the vertical axis represent the relative expression against actin beta, calculated using the  $2^{-\Delta\text{CT}}$  method. The data represent the mean  $\pm$  standard deviation of three independent experiments.

**FIGURE 4** Morphological phenotypes of Chediak-Higashi syndrome induced pluripotent stem cell-derived myeloid cells. (a) Schematic diagram of the myeloid cell differentiation and analysis. (b) Representative images of myeloid cells derived from pluripotent stem cells (PSCs). Left: May-Grunwald Giemsa staining. Right: Myeloperoxidase (MPO) staining. Bars = 10  $\mu\text{m}$ . (c) Quantification of cytosolic granules calculated from the images shown in (b). In the box and whisker plot, boxes extend from the first to the third quartile, and the lines inside the boxes indicate the median. Upper and lower whiskers represent the 95% percentile and 5% percentiles respectively, of 300 cells from 3–5 independent biological replicates each. Individual data points between the 95 and 100 percentiles or the 0 and 5 percentiles are outliers and plotted individually. (d) MPO electron microscopy images of PSC-derived myeloid cells (day 25). Statistical analysis was performed using the Kruskal-Wallis one-way analysis of variance with Dunn's multiple comparisons test. \* $p < 0.0001$ .



controls.<sup>35</sup> Additionally, the same cells have been reported to contain giant and normal-sized granules.<sup>33</sup> The reason some cells with *LYST* mutations retain

normal granule cells is not clear. The behavior of lysosomes and endosomes and intracellular stress may affect the granule size, but another possibility is that

the expression level of *LYST* may be variable in each cell. In any case, such a wide variation in granule size indicates that it is not easy to construct a high-throughput screening (HTS) system using granule size as an indicator. Although phenotype-based HTS using patient-derived iPSCs is an innovative tool for drug discovery,<sup>19</sup> in the case of CHS, other quantitative phenotypes, such as the expression level of *LYST* or the function of granules, should be considered.

Hemophagocytic lymphohistiocytosis is a serious life-threatening event in CHS. Currently, the primary trigger of HLH is thought to be the loss of cytotoxicity in CTLs and NK cells,<sup>36</sup> which causes prolonged cell-to-cell interactions with antigen-presenting cells, resulting in a proinflammatory cytokine storm and subsequent macrophage activation. Macrophages, one of the representative myeloid cells, also play an important role in HLH to complete its phenotype by producing proinflammatory cytokines and phagocytosing hematopoietic cells.<sup>36</sup> On the other hand, the role of neutrophils on HLH has not been fully elucidated. However, neutrophils in familial hemophagocytic lymphohistiocytosis (FHL) type 5 syndrome caused by *STXBP2/Munc18-2* mutation showed a profound defect in granule mobilization,<sup>37</sup> which may be associated with persistent inflammation. Considering that the abnormal persistence of tissue inflammatory immune responses contributes to the development of HLH, the impaired neutrophil granule mobilization observed in FHL, including CHS, may be associated with the pathogenesis of HLH. Given our finding that the phenotype was confirmed in iPSC-derived myeloid cells, deriving the hematopoietic cells responsible for HLH i.e. macrophages,<sup>29</sup> NK cells<sup>38,39</sup> and CTLs,<sup>40</sup> from iPSCs may help clarify the mechanisms and identify treatments for HLH. CHS-iPSCs are also useful for constructing in vitro models of extra-hematopoietic lesions such as neurons and melanocytes.

In conclusion, we established iPSCs from two CHS patients and succeeded in reproducing a characteristic cellular phenotype, giant granules, by differentiating them into myeloid cells. This finding demonstrates that iPSCs are useful for elucidating the pathogenesis of CHS patients. iPSC-based disease models offer a useful option for clarifying the pathogenesis of and developing treatments for symptoms that persist after HSCT, such as neurological deficits and oculocutaneous albinism.

#### AUTHOR CONTRIBUTIONS

Shigeharu Oh, Akira Niwa, Tatsutoshi Nakahata, and Megumu K. Saito designed the study. Shigeharu Oh and Ayako Nagahashi performed the experiments. Shigeharu Oh, Akira Niwa, Isao Asaka, and Tatsutoshi Nakahata collected and analyzed the data. Shigeharu Oh, Akira Niwa, and Megumu K. Saito wrote the manuscript. Tatsutoshi Nakahata provided

conceptual advice. All authors read and approved the final manuscript.

#### ACKNOWLEDGMENTS

We thank the recruited CHS patients for participating in this study, Ms. Harumi Watanabe for administrative assistance, Mr. Ryunosuke Ikeda for technical assistance, Dr. Mitsuaki Kimura for donor recruiting, Dr. Peter Karagiannis for proofreading the paper, Dr. Hiroyuki Matsubara for the randomization of myeloperoxidase preparations, Dr. Shinya Yamanaka for providing a control iPSC line, Dr. Norio Nakatsuji for providing an ESC line, KhESI, Dr. Keiko Okamoto-Furuta, Dr. Haruyasu Kohda (Center for Anatomical Study, Kyoto University) for the preparations of the MPO electron microscopy, Dr. Keisuke Okita for providing plasmid vectors, and Dr. Naoya. M. Suzuki for performing the teratoma assay. This work was supported by the Japan Society for the Promotion of Science (JSPS) KAKENHI (20H03642) to M.K.S., the grant for the Core Center for iPSC Cell Research of Research Center Network for Realization of Regenerative Medicine (JP21bm0104001) from the Japan Agency for Medical Research and Development (AMED) to M.K.S., and the Program for Intractable Diseases Research utilizing Disease-specific iPSC cells of AMED (21bm0804004 and JP19bm0804001) to M.K.S.

#### CONFLICT OF INTEREST

The authors declare no conflicts of interest.

#### ORCID

Akira Niwa  <https://orcid.org/0000-0002-6412-2686>  
Megumu K. Saito  <https://orcid.org/0000-0001-8813-3614>

#### REFERENCES

- Barbosa MD, Nguyen QA, Tchernev VT, Ashley JA, Detter JC, Blydes SM, et al. Identification of the homologous beige and Chediak-Higashi syndrome genes. *Nature*. 1996;382(6588):262–5.
- Nagle DL, Karim MA, Woolf EA, Holmgren L, Bork P, Misumi DJ, et al. Identification and mutation analysis of the complete gene for Chediak-Higashi syndrome. *Nat Genet*. 1996;14(3):307–11.
- Perou CM, Moore KJ, Nagle DL, Misumi DJ, Woolf EA, McGrail SH, et al. Identification of the murine beige gene by YAC complementation and positional cloning. *Nat Genet*. 1996;13(3):303–8.
- Holland P, Torgersen ML, Sandvig K, Simonsen A. *LYST* affects lysosome size and quantity, but not trafficking or degradation through autophagy or endocytosis. *Traffic*. 2014;15(12):1390–405.
- Sepulveda FE, Burgess A, Heiligenstein X, Goudin N, Ménager MM, Romao M, et al. *LYST* controls the biogenesis of the endosomal compartment required for secretory lysosome function. *Traffic*. 2015;16(2):191–203.
- Westphal A, Cheng W, Yu J, Grassl G, Krautkrämer M, Holst O, et al. Lysosomal trafficking regulator *Lyst* links membrane trafficking to toll-like receptor-mediated inflammatory responses. *J Exp Med*. 2016;214(1):227–44.

7. Hansson M, Olsson I, Nauseef W. Biosynthesis, processing, and sorting of human myeloperoxidase. *Arch Biochem Biophys.* 2006;445:214–24.
8. Higashi O. Congenital abnormality of peroxidase granules; a case of congenital gigantism of peroxidase granules, preliminary report. *Tohoku J Exp Med.* 1953;58(3–4):246.
9. Canna SW, Marsh RA. Pediatric hemophagocytic lymphohistiocytosis. *Blood.* 2020;135(16):1332–43.
10. Nagai K, Ochi F, Terui K, Maeda M, Ohga S, Kanegane H, et al. Clinical characteristics and outcomes of Chédiak-Higashi syndrome: a nationwide survey of Japan. *Pediatr Blood Cancer.* 2013;60(10):1582–6.
11. Dotta L, Parolini S, Prandini A, Tabellini G, Antolini M, Kingsmore SF, et al. Clinical, laboratory and molecular signs of immunodeficiency in patients with partial oculo-cutaneous albinism. *Orphanet J Rare Dis.* 2013;17(8):168.
12. Cooper N, Rao K, Gilmour K, Hadad L, Adams S, Cale C, et al. Stem cell transplantation with reduced-intensity conditioning for hemophagocytic lymphohistiocytosis. *Blood.* 2006;107(3):1233–6.
13. Eapen M, DeLaat CA, Baker KS, Cairo MS, Cowan MJ, Kurtzberg J, et al. Hematopoietic cell transplantation for Chediak-Higashi syndrome. *Bone Marrow Transplant.* 2007;39(7):411–5.
14. Haddad E, Le Deist F, Blanche S, Benkerrou M, Rohrlach P, Vilmer E, et al. Treatment of Chediak-Higashi syndrome by allogeneic bone marrow transplantation: report of 10 cases. *Blood.* 1995;85(11):3328–33.
15. Umeda K, Adachi S, Horikoshi Y, Imai K, Terui K, Endo M, et al. Allogeneic hematopoietic stem cell transplantation for Chediak-Higashi syndrome. *Pediatr Transplant.* 2016;20(2):271–5.
16. Tardieu M, Lacroix C, Neven B, Bordigoni P, de Saint Basile G, Blanche S, et al. Progressive neurologic dysfunctions 20 years after allogeneic bone marrow transplantation for Chediak-Higashi syndrome. *Blood.* 2005;106(1):40–2.
17. Prieur DJ, Collier LL. Animal model of human disease: Chédiak-Higashi syndrome. *Am J Pathol.* 1978;90(2):533–6.
18. Mestas J, Hughes CC. Of mice and not men: differences between mouse and human immunology. *J Immunol.* 2004;172(5):2731–8.
19. Karagiannis P, Takahashi K, Saito M, Yoshida Y, Okita K, Watanabe A, et al. Induced pluripotent stem cells and their use in human models of disease and development. *Physiol Rev.* 2019;99(1):79–114.
20. Karagiannis P, Yamanaka S, Saito MK. Application of induced pluripotent stem cells to primary immunodeficiency diseases. *Exp Hematol.* 2019;71:43–50.
21. Aarts CEM, Varga E, Webbers S, Geissler J, von Lindern M, Kuijpers TW, et al. Generation and characterization of a human iPSC line SANi008-a from a Chédiak-Higashi syndrome patient. *Stem Cell Res.* 2021;55:102442.
22. Mica Y, Lee G, Chambers SM, Tomishima MJ, Studer L. Modeling neural crest induction, melanocyte specification, and disease-related pigmentation defects in hESCs and patient-specific iPSCs. *Cell Rep.* 2013;3(4):1140–52.
23. Serra-Vinardell J, Sandler MB, Pak E, Zheng W, Dutra A, Introne W, et al. Generation and characterization of four Chediak-Higashi syndrome (CHS) induced pluripotent stem cell (iPSC) lines. *Stem Cell Res.* 2020;22(47):101883.
24. Takahashi K, Tanabe K, Ohnuki M, Narita M, Ichisaka T, Tomoda K, et al. Induction of pluripotent stem cells from adult human fibroblasts by defined factors. *Cell.* 2007;131(5):861–72.
25. Tanabe F, Kasai H, Morimoto M, Oh S, Takada H, Hara T, et al. Novel heterogenous CHS1 mutations identified in five Japanese patients with Chediak-Higashi syndrome. *Case Rep Med.* 2010;2010:1, 464671–5.
26. Okita K, Matsumura Y, Sato Y, Okada A, Morizane A, Okamoto S, et al. A more efficient method to generate integration-free human iPSCs. *Nat Methods.* 2011;8:409–12.
27. Tanaka T, Takahashi K, Yamane M, Tomida S, Nakamura S, Oshima K, et al. Induced pluripotent stem cells from CINCA syndrome patients as a model for dissecting somatic mosaicism and drug discovery. *Blood.* 2012;120(6):1299–308.
28. Niwa A, Heike T, Umeda K, Oshima K, Kato I, Sakai H, et al. A novel serum-free monolayer culture for orderly hematopoietic differentiation of human pluripotent cells via mesodermal progenitors. *PLoS One.* 2011;6(7):e22261.
29. Yanagimachi MD, Niwa A, Tanaka T, Honda-Ozaki F, Nishimoto S, Murata Y, et al. Robust and highly-efficient differentiation of functional monocytic cells from human pluripotent stem cells under serum- and feeder cell-free conditions. *PLoS One.* 2013;8(4):e59243.
30. Nakagawa M, Taniguchi Y, Senda S, Takizawa N, Ichisaka T, Asano K, et al. A novel efficient feeder-free culture system for the derivation of human induced pluripotent stem cells. *Sci Rep.* 2014;8(4):3594.
31. Okita K, Yamakawa T, Matsumura Y, Sato Y, Amano N, Watanabe A, et al. An efficient nonviral method to generate integration-free human-induced pluripotent stem cells from cord blood and peripheral blood cells. *Stem Cells.* 2013;31(3):458–66.
32. White JG, Clawson CC. The Chédiak-Higashi syndrome: ring-shaped lysosomes in circulating monocytes. *Am J Pathol.* 1979;96(3):781–98.
33. White JG, Krumwiede M. Normal-sized primary lysosomes are present in Chediak-Higashi syndrome neutrophils. *Pediatr Res.* 1987;22(2):208–15.
34. Chiang SCC, Wood SM, Tesi B, Akar HH, Al-Herz W, Ammann S, et al. Differences in granule morphology yet equally impaired exocytosis among cytotoxic T cells and NK cells from Chediak-Higashi syndrome patients. *Front Immunol.* 2017;18(8):426.
35. Abe K, Arashima S, Honma M. Distribution pattern of lysosomal granules in fibroblasts of the Chediak-Higashi syndrome. *J Clin Pathol.* 1982;35(5):496–501.
36. Crayne CB, Albeituni S, Nichols KE, Cron RQ. The immunology of macrophage activation syndrome. *Front Immunol.* 2019;10:119.
37. Zhao XW, Gazendam RP, Drewniak A, van Houdt M, Tool ATJ, van Hamme JL, et al. Defects in neutrophil granule mobilization and bactericidal activity in familial hemophagocytic lymphohistiocytosis type 5 (FHL-5) syndrome caused by STXBP2/Munc18-2 mutations. *Blood.* 2013;122(1):109–11.
38. Knorr DA, Ni Z, Hermanson D, Hexum MK, Bendzick L, Cooper LJ, et al. Clinical-scale derivation of natural killer cells from human pluripotent stem cells for cancer therapy. *Stem Cells Transl Med.* 2013;2(4):274–83.
39. Matsubara H, Niwa A, Nakahata T, Saito MK. Induction of human pluripotent stem cell-derived natural killer cells for immunotherapy under chemically defined conditions. *Biochem Biophys Res Commun.* 2019;515(1):1–8.
40. Nishimura T, Kaneko S, Kawana-Tachikawa A, Tajima Y, Goto H, Zhu D, et al. Generation of rejuvenated antigen-specific T cells by reprogramming to pluripotency and redifferentiation. *Cell Stem Cell.* 2013;12(1):114–26.

## SUPPORTING INFORMATION

Additional supporting information can be found online in the Supporting Information section at the end of this article.

**How to cite this article:** Oh S, Niwa A, Nagahashi A, Asaka I, Nakahata T, Saito MK. iPSC cells from Chediak-Higashi syndrome patients recapitulate the giant granules in myeloid cells. *Pediatr Int.* 2022;64:e15390. <https://doi.org/10.1111/ped.15390>